

## Accepted Manuscript

A molecular dynamics study of the force between planar substrates due to capillary bridges

J.H. Saavedra, R.E. Rozas, P.G. Toledo

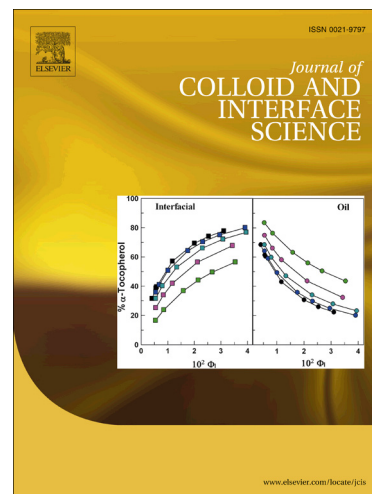
PII: S0021-9797(14)00177-5  
DOI: <http://dx.doi.org/10.1016/j.jcis.2014.03.050>  
Reference: YJCIS 19469

To appear in: *Journal of Colloid and Interface Science*

Received Date: 8 October 2013  
Accepted Date: 20 March 2014

Please cite this article as: J.H. Saavedra, R.E. Rozas, P.G. Toledo, A molecular dynamics study of the force between planar substrates due to capillary bridges, *Journal of Colloid and Interface Science* (2014), doi: <http://dx.doi.org/10.1016/j.jcis.2014.03.050>

This is a PDF file of an unedited manuscript that has been accepted for publication. As a service to our customers we are providing this early version of the manuscript. The manuscript will undergo copyediting, typesetting, and review of the resulting proof before it is published in its final form. Please note that during the production process errors may be discovered which could affect the content, and all legal disclaimers that apply to the journal pertain.



## A molecular dynamics study of the force between planar substrates due to capillary bridges

J.H. Saavedra<sup>a</sup>, R.E. Rozas<sup>b</sup>, P.G. Toledo<sup>a,\*</sup><sup>a</sup>Chemical Engineering Department and Surface Analysis Laboratory (ASIF), University of Concepción, PO Box 160-C, Correo 3, Concepción, Chile<sup>b</sup>Institut für Theoretische Physik der Weichen Materie, Heinrich Heine-Universität Düsseldorf, Universitätsstraße 1, 40225 Düsseldorf, Germany**Abstract**

Molecular dynamics simulations are used to study capillary liquid bridges between two planar substrates and the origin, strength and range of the resulting force between them. Pairwise interactions are described by the Lennard-Jones potential. Surface wettability is tuned by varying the fluid-substrate well depth interaction parameter. The force between the substrates due to a bridge of liquid is estimated by different methods including non-equilibrium simulations of moving substrates connected by liquid bridges and macroscopic balance of forces. The latter involves knowledge of liquid-vapor interfacial free energy, curvature radii, radius of wetted area and contact angle at the triple-phase contact line. All these physical quantities are estimated from equilibrium simulations. The force is attractive when the substrates are solvophilic or moderately solvophobic; and thus for cavities surrounded by the same liquid the force is attractive even when the substrates are moderately solvophilic. Two threshold values for the fluid-substrate potential interaction parameter can be identified; one for which the effective interaction between substrates due to liquid bridges changes from repulsive to attractive and another for which the capillary bridge becomes mechanically unstable and breaks into droplets.

**Keywords:** Capillary bridge, hydrophilic-hydrophobic interaction, long-range forces, molecular dynamics, confined liquids

**1. Introduction**

Molecular simulations have been used to study the behavior of fluids confined between substrates and also the wetting behavior of liquid drops and nuclei on solid substrates but not, to the best of our knowledge, the nature and range of the resulting force between the surfaces for different wettability conditions. The wetting of the liquid phase, droplets or bridges, is set by the strength of the interaction between particles in the fluid and in the substrate. Strong fluid-solid interactions lead to lower contact angles, measured through the liquid phase, and thus to higher wettability.

Molecular dynamics was used early by Koplik *et al.* [1] to study microscopic aspects of slow viscous flows past a solid wall, where both fluid and wall have molecular structure. They also simulated an immiscible two-fluid system and were able to vary the interaction between the fluids and the wall. A static meniscus was observed whose contact angle agrees with estimates from the Young equation and, when motion occurs, advancing and receding contact angles were observed. Although solid-fluid interaction was not explored thoroughly, partial results indicate that contact angle, measured through the wetting phase, decreases as the interaction increases. Later, Busic *et al.* [2] studied by molecular dynamics simulations the extensional rheology of Newtonian and non-Newtonian fluid bridges between two substrates. The evolution of the liquid filament profile and the forces exerted on the end-plates obtained from the simula-

tions, and also the internal dynamics of the fluid and the molecular configurations, were in good agreement with experimental data and with results from macroscopic numerical calculations. Koplik and Banavar [3] presented molecular dynamics simulations of filaments of a non-Newtonian liquid stretched under uniaxial deformation to the point of breaking. They observed non-uniform extensions leading to highly uneven shapes and alternating stretched and unstretched regions of liquid. Bucior *et al.* [4] used non-equilibrium molecular dynamics to investigate the kinetics aspects of the evaporation of liquid bridges confined between walls for different wetting conditions to elucidate the effect of the capillary inhomogeneity on this process.

Concerning simulation studies of the three-phase contact of equilibrated liquid droplets/bridges with substrates two main approaches are commonly used to determine the contact angle from simulations; in one method the liquid or droplet is prepared and the angle is obtained from averaged density profiles, in the other, the Young equation is used to estimate the angle and the involved interfacial free energies  $\gamma_{AB}$  are determined separately. Both methods have been also used in combination to test the consistency of the results. Maruyama *et al.* [5] used molecular dynamics simulations to study a Lennard-Jones liquid droplet on a solid substrate made of particles pinned to fcc lattice points by harmonic springs and applied the same methodology to study droplets of water on platinum fcc substrates [6]. They found that the contact angle depends on the crystalline orientation of the substrate being larger for fcc(100), intermediate for fcc(111) and lower for fcc(110). Shi and Dir [7] obtained contact angles from density profiles of a Lennard-Jones liquid droplet on a Lennard-Jones substrate at different

\*Corresponding author

Email address: petoledo@udec.cl (P.G. Toledo)

temperatures and wetting conditions and also studied the effect of temperature over the contact angle of water over platinum. The role of the substrate-fluid interaction strength and substrate topographies was investigated by Leroy and Müller-Plathe [8] using molecular dynamics simulations. The contact angles were directly determined from density profiles, the solid-liquid and liquid-vapor interfacial free energies were respectively determined from thermodynamic integration method and from the anisotropy of the pressure tensor at the interface. The simulation results showed that the contribution of the solid-vapor interfacial free energy in the Young equation is small when the solid-liquid interaction is weak. Semirami and Azimian [9] studied the effect of temperature and solid-fluid interaction on the wetting of a Lennard-Jones system. A common result of these works is the lowering of the contact angle as the solid-fluid interaction parameter increases. An alternative approach was applied by Grzelak and Errington [10] to determine contact angle, solid-vapor and solid-liquid interfacial tensions. The method is based on biased grand canonical Monte Carlo simulation which provides the dependence of the interfacial free energy on density (for a description of the method see also [11–13]). Their results show good agreement with those obtained from the mechanical definition of interfacial tension. Das and Binder [14] used Monte Carlo simulations to investigate a immiscible binary Lennard-Jones fluid between walls, a system where bridges rich in one of the components are formed. They evaluated contact angles and interfacial free energies separately for different wall-fluid interaction strengths and showed that the Young’s equation applies at the nanoscale. Here we use molecular dynamics simulations of nanoscopic capillary liquid bridges between planar substrates to determine the resulting force between the substrates. The wettability is tuned by varying the solid-fluid interaction parameter. The force between the substrates is estimated from different methods; (i) from a macroscopic force balance, where the physical quantities involved are determined from equilibrium simulations (ii) by applying second Newton’s law to moving substrates connected by liquid bridges, and (iii) from the integration of the normal pressure radial profile of equilibrated liquid bridges.

## 2. Methods

Molecular dynamics simulations of liquid capillary bridges connecting two substrates are performed. Equations of motion are solved with the velocity Verlet algorithm [15] and particle interactions are modeled with the 12-6 Lennard-Jones potential [16] truncated and shifted at a cut-off distance of  $2.5\sigma_{ij}$  with  $i$  and  $j$  denoting particles in the fluid (f) or in the substrate (s). The following reduced units are used; for length  $L^* = L/\sigma_f$ , time  $t^* = (t/\sigma_f)(\epsilon_f/m_f)^{1/2}$ , mass  $m^* = m/m_f$  and temperature  $T^* = k_B T/\epsilon_f$ . The interaction parameters for particles in the fluid are  $\sigma_f^* = 1$  and  $\epsilon_f^* = 1$ , for particles in the substrate  $\sigma_s^* = 1$  and  $\epsilon_s^* = 10$ , and for the substrate-fluid particle interaction  $\sigma_{sf}^* = 1$  and variable well depth  $\epsilon_{sf}^*$  in order to attain different wetting conditions. The particle masses are  $m_f^* = 1$  and  $m_s^* = 10$ . The integration time step is  $t^* = 0.0023$ .

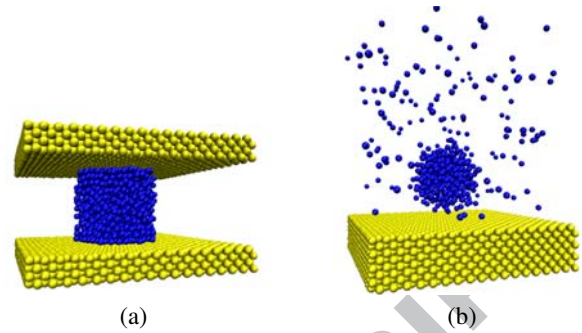


Figure 1: Snapshots of initial configurations for simulations of (a) a liquid bridge between two planar substrates and (b) a liquid droplet over a flat substrate.

### 2.1. Preparation of a capillary bridge

The substrate and the fluid are prepared in independent simulations and then put in contact. An fcc crystalline substrate of 4 atom layers thickness and initial lateral lengths  $L_x^* = L_y^* = 30$  is relaxed in an  $NPT$  simulation at  $T^* = 0.68$  and  $P^* = 0$  (condition for which the fcc phase is stable). Then two copies of the equilibrated substrates are disposed in a simulation box at a distance  $D^*$  along the direction perpendicular to the substrate surface  $z$ . The crystalline orientation of the surface is fcc(100). The positions of the particles in the first external layer are fixed in both substrates and the system is equilibrated in an  $NVT$  simulation. A liquid is prepared in an  $NVT$  simulation in a box of lengths  $L_x^* \times L_y^* \times (D^* - 2)$  using periodic boundaries in all directions. In the next step the liquid is disposed in the volume between the substrates and the system is equilibrated in  $NVT$  simulation over  $2 \cdot 10^5$  time steps. Finally, in order to create a bridge, the particles in the liquid outside a cylinder of radius  $R^*$  are removed. The remaining number of particles in the bridge are  $N = 941$  and its nominal dimensions are  $R^* = 5.9$  and  $D^* = 10.8$  (see Figure 1a). The resulting system is equilibrated in an  $NVT$  simulation during  $10^6$  time steps. The temperature is kept constant with a Berendsen thermostat with a relaxation time  $\tau^* = 0.46$ .

### 2.2. Preparation of a liquid droplet

Simulations of a liquid droplet over a single substrate are used to assess the contact angle given  $T^*$  and  $\epsilon_{sf}^*$  for comparison with results from simulation of a bridge with the same Lennard Jones potential and parameters. A substrate of 8 layers and initial lateral lengths  $L_x^* = L_y^* = 30$  is prepared in an  $NPT$  simulation at  $T^* = 0.68$  and  $P^* = 0$ . As for bridges the fcc(100) surface crystalline orientation is considered. The droplet is obtained from an independent simulation and then is located over the substrate along the  $z$ -axis. First, a system made of 500 particles at  $T^* = 1.30$  and liquid density is equilibrated inside a periodic cubic simulation box. Later, the box is expanded to obtain a liquid droplet. After  $2 \cdot 10^6$  time steps a liquid droplet in equilibrium with its vapor is obtained. Particles that belong to the droplet are identified according to the Stillinger criterion [17] for a threshold radius of 1.5. The droplet and its vapor are then displaced so that the lowest particle belonging to the droplet is

located right at the bottom of the simulation box. Vapor particles below this limit appear at the top of the box by virtue of a periodic boundary at the bottom of the box. Then, the drop is aligned over the substrate with a gap of  $\sigma_f^*$  to avoid particle overlapping but enough to guarantee interaction between the substrate and the liquid droplet. To keep the substrate particles in their positions, the layer located at the bottom of the  $z$ -axis is kept fixed at its position. Periodic boundary conditions are applied in the  $x$  and  $y$  directions, and a reflective wall is located at the upper boundary in the  $z$ -axis. Finally, from this last configuration (see Figure 1b) the entire system is equilibrated during  $4 \cdot 10^6$  time steps at  $T^* = 0.68$  for different values of  $\epsilon_{sf}^*$ . The Berendsen thermostat is used with a relaxation time  $\tau^* = 0.46$ .

### 2.3. Liquid-vapor interfacial free energy

The liquid-vapor interfacial free energy is obtained from molecular dynamics simulations of a planar liquid film in contact with its vapor. The system considered here contains 5324 fluid particles at  $T^* = 0.68$ . The interfacial tension is estimated from the integration of the difference between the normal and tangential pressure profiles along the liquid-vapor interface. The Irving-Kirkwood definition of the local pressure component is adopted [18, 19].

### 2.4. Contact angle and curvature radii of a bridge

Two-dimensional density profiles from equilibrated simulations are used to characterize capillary bridges. Time average over 4000 configurations is considered to calculate the profiles. The instantaneous center of mass of the bridges is corrected in directions  $x$  and  $y$  in a way that such center is located at the center of the simulation box  $(x^*, y^*) = (0, 0)$ . Contact angle  $\theta$ , azimuthal curvature radius  $R_1^*$ , meridional curvature radius  $R_2^*$  and radius of the wetted area  $R^*$  are determined by adjusting a circle to the contour line of the liquid-vapor interface of the bridge corresponding to the average density between the liquid (l) and the vapor (v) bulk densities,  $\rho_{lv}^*(r^*, z^*) = (\rho_f^* - \rho_v^*)/2$ . The first fluid layer in contact with the substrate is ignored in the fit of the profile contour. Figure 2 illustrates the procedure where the radial coordinate is defined as  $r^{*2} = x^{*2} + y^{*2}$ . The adjustment of the circle  $(r^* - r_0^*)^2 + z^{*2} = R_1^{*2}$  in Figure 2 provides directly the center of the circle  $(r^*, z^*) = (r_0^*, 0)$  and the azimuthal curvature radius  $R_1^*$ . The meridional curvature radius is equal to  $R_2^* = r_0^* \pm R_1^*$  and the radius of the wetted area to  $R^* = r_0^* \pm (R_1^{*2} - z_p^{*2})^{1/2}$ , where  $z_p^*$  corresponds to the position of the plane parallel to the substrate where the contact angle is evaluated. Here we use  $z_p^* = -4.3$ , i.e. located between the first and the second layer of liquid near the substrates, as shown in Figure 2. The contact angle is obtained from the slope of the line tangent to the fit function  $z^*(r^*)$  at the contact plane  $z^* = z_p^*$  according to  $\tan \theta = -m$  when  $\theta < 90^\circ$  and  $\tan(180^\circ - \theta) = +m$  when  $\theta > 90^\circ$  with  $m = (dz^*/dr^*)_{z^*=z_p^*}$ .

## 3. Results and discussion

### 3.1. Characterization of capillary bridges

The methodology for preparing capillary bridges previously described leads to stable liquid bridges for  $\epsilon_{sf}^*$  between 0.1 and

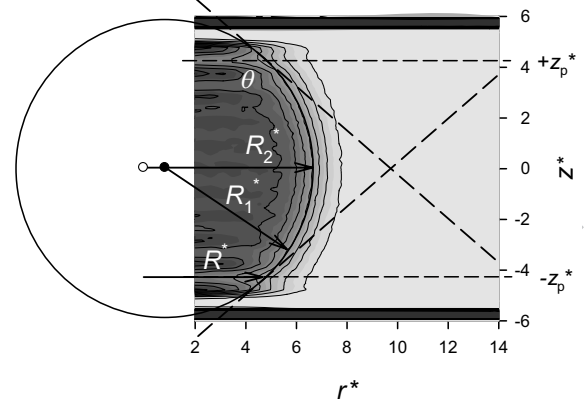


Figure 2: Curvature radii  $R_1^*$  and  $R_2^*$ , radius of wetted area  $R^*$ , and contact angle  $\theta$  determination from a two-dimensional density profile for  $\epsilon_{sf}^* = 0.2$ . Dashed lines correspond to tangent lines at the three-phase contact lines. The first fluid layer in contact with the substrate is ignored in the fit of the profile contour. The black dot represents the location of the center of the circle  $(r_0^*, 0)$ , and the white dot represents the location of the center of the bridge  $(0, 0)$ .

Table 1: Curvature radii  $R_1^*$ , radius of wetted area  $R_2^*$  and contact angle at triple-phase contact line  $\theta$  for equilibrated capillary bridges between planar substrates at  $T^* = 0.68$  and different  $\epsilon_{sf}^*$ .

$\epsilon_{sf}^*$	$R_1^*$	$R_2^*$	$R^*$	$\theta^\circ$
0.1	4.9	6.8	4.3	151
0.2	5.7	6.6	4.7	139
0.3	7.7	6.3	5.0	124
0.4	14.2	6.0	5.3	108
0.5	$\infty$	5.7	5.6	90
0.6	-13.6	5.2	5.9	72
0.7	-6.5	4.4	6.0	49

0.7. Initial cylinder radius is  $R_0^* = 5.9$ , number of particles is  $N = 941$ , and separation distance between the surfaces is  $D^* = 10.8$ . Both the simulation snapshots in Figure 3 and the averaged two-dimensional density profiles shown in Figure 4 clearly show the increasing affinity of the liquid for the substrate as  $\epsilon_{sf}^*$  increases. For  $\epsilon_{sf}^* < 0.5$ , the three-phase contact line is very well defined and thus estimating the value of the contact angle is simple. For  $\epsilon_{sf}^* = 0.5$ , the spreading of the liquid bridge is accompanied by the formation of a thin liquid layer at the fluid-substrate contact region, yet calculating the contact angle is possible by neglecting this thin liquid layer. For  $0.6 < \epsilon_{sf}^* < 0.7$  the spreading of the liquid droplet is accompanied by a thin film of significant lateral extent. For  $\epsilon_{sf}^* > 0.8$  wetting is so strong that a stable bridge is not possible. The liquid bridges are characterized in terms of their contact angles and curvature radii which are calculated from the density profiles shown in Figure 4. Table 1 summarizes azimuthal and meridional radii of curvature, radius of the wetted area by the bridge, and contact angles at the triple-phase contact lines for different values of  $\epsilon_{sf}^*$ . Contact angles decrease as  $\epsilon_{sf}^*$  increases. The azimuthal radius of curvature is positive when

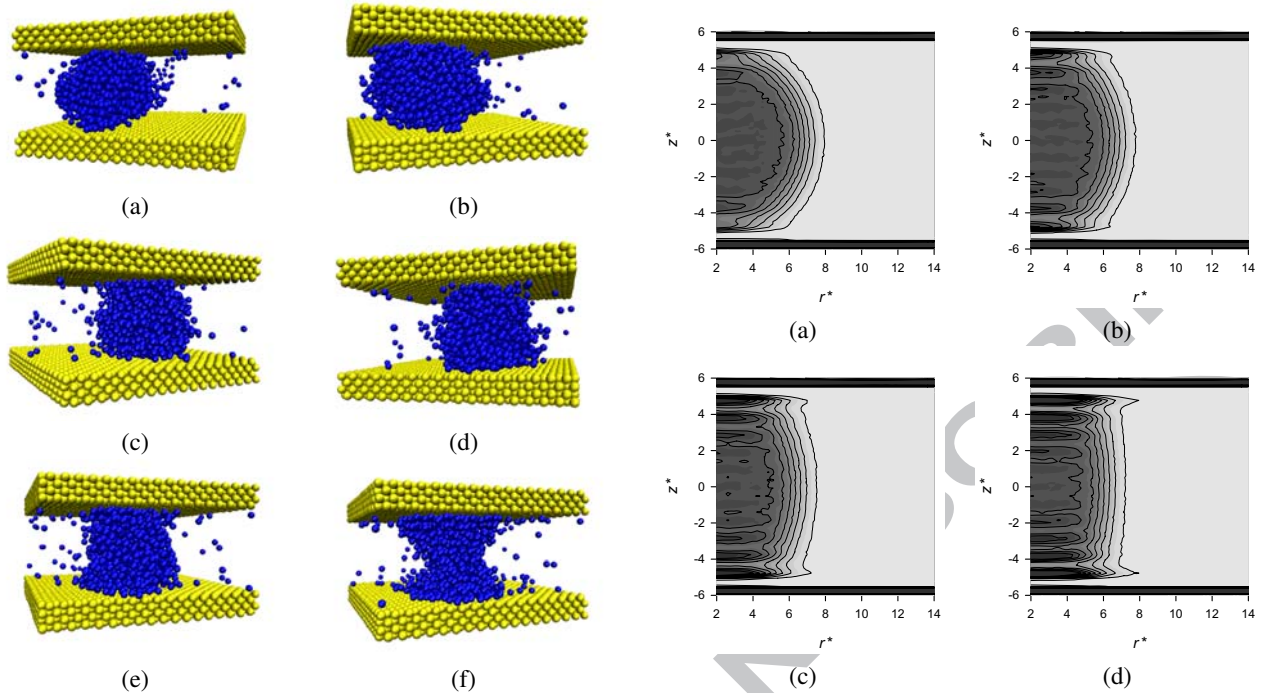


Figure 3: Snapshots of capillary bridges of liquid (blue) equilibrated between two substrates (yellow) at  $T^* = 0.68$ ,  $N_f$  and several  $\epsilon_{sf}^*$  (a) 0.1, (b) 0.2, (c) 0.3, (d) 0.4, (e) 0.5 and (f) 0.7. Distance between substrates is  $D^* = 10.8$  in all simulations.

measured from the inside of the bridge, the case for example of a capillary bridge of water between hydrophobic surfaces, and negative when measured from outside the bridge, the case for example of a capillary bridge of water between hydrophilic surfaces. Figure 5 shows the dependence of the contact angle with  $\epsilon_{sf}^*$  for liquid droplets and capillary bridges. Results for droplets are for a system with 500 particles, increasing the size of the system to 864 particles did not change results significantly. Results for liquid bridges are for a system with 941 particles. Contact angles of bridges and droplets coincide for  $\epsilon_{sf}^* < 0.6$ . For  $\epsilon_{sf}^* > 0.6$  the contact angle for droplets are larger than for bridges. In Figure 5 our contact angles for bridges and droplets are compared with results reported in the literature. Contact angles always decreases when  $\epsilon_{sf}^*$  increases. For  $\epsilon_{sf}^* < 0.5$ , which defines a non-wetting ( $\theta \rightarrow 180^\circ$ ) to neutral wetting ( $\theta \rightarrow 90^\circ$ ) domain, there is good agreement in general although the systems may be significantly different. In these domains, cohesive forces dominate over adhesive forces and thus the interaction between particle pairs is stronger than between fluid and solid particles. As the contact angle is sensitive to the cross interactions then such differences in the systems do not appear in Figure 5. Situation is the opposite for  $\epsilon_{sf}^* > 0.5$ , which defines a wetting ( $\theta \rightarrow 0^\circ$ ) domain. In this domain adhesive forces are stronger than cohesive forces and thus the cross interaction between fluid and solid particles sets the wetting degree. Cross interactions and contact angles that arise depend on the characteristics of each system and hence it is expected that the differences between systems appear reflected in Figure 5.

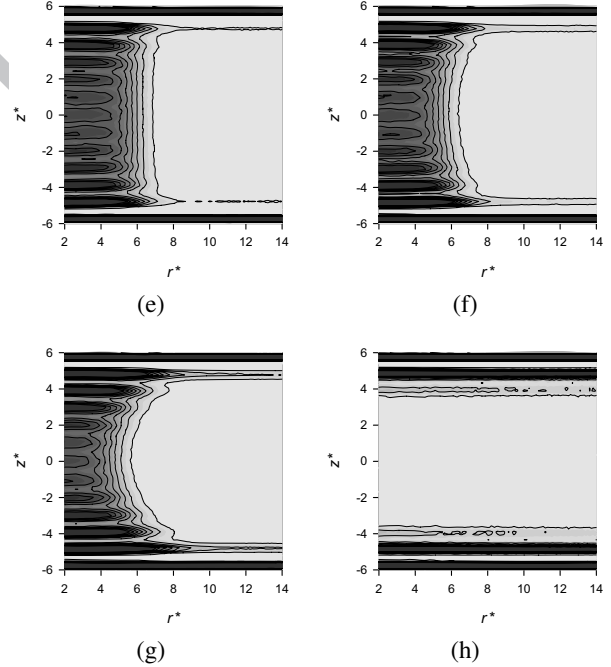


Figure 4: Averaged two dimensional density profiles for equilibrated liquid bridges between two substrates at  $T^* = 0.68$  and different  $\epsilon_{sf}^*$  (a) 0.1, (b) 0.2, (c) 0.3, (d) 0.4, (e) 0.5, (f) 0.6, (g) 0.7 and (h) 0.9. Distance between substrates is  $D^* = 10.8$  in all simulations.

To this point we have characterized capillary bridges of liquid through two dimensional density profiles, contact angles, curvature radii and radius of wetted area. With this information in hand it is possible to estimate the force between the two surfaces connected by a bridge. The distance between the surfaces

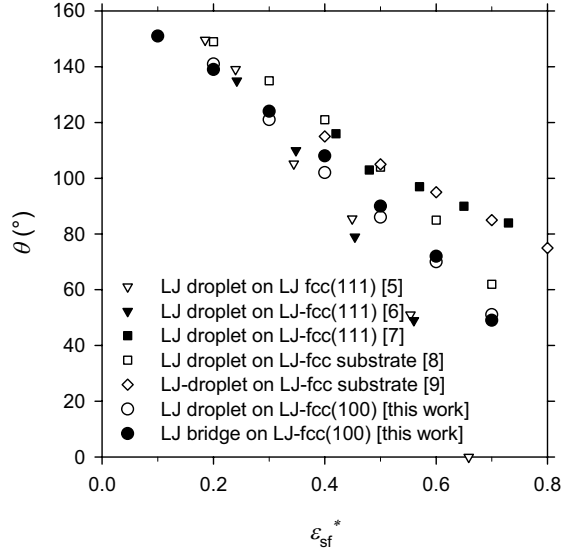


Figure 5: Contact angles measured for liquid droplets (black circles) and capillary bridges (white circles) as function of the solid-fluid interaction parameter  $\epsilon_{sf}^*$ . Our values are compared with previous literature results.

is larger than the interaction cut-off diameter so that no direct force exists between them.

### 3.2. Forces between substrates connected by a capillary bridge

The force between two surfaces connected by a capillary bridge can be obtained from a macroscopic force balance and from molecular dynamics data. Here we compare both.

#### 3.2.1. Macroscopic force balance

The force between two identical planar surfaces connected by a capillary bridge can be rationalized as the contribution of the force due to the surface tension and the force due to the difference of pressure between the bridge and the surrounding medium. Eq. (1) includes both contributions when applied to the triple-phase contact line.

$$F^* = -2\pi R^* \gamma_{lv}^* \sin \theta + \pi R^{*2} \gamma_{lv}^* \left( \frac{1}{R_1^*} + \frac{1}{R_2^*} \right) \quad (1)$$

The first term in the right side of Eq. (1) corresponds to the attractive contribution of the surface tension and the second to the contribution of the pressure difference.  $R^*$ ,  $R_1^*$  and  $R_2^*$  represent respectively the radius of the wetted area by the bridge, and the azimuthal and meridional radii of curvature of the bridge (see Figure 2). This equation can be applied to a bridge of liquid surrounded by a gas or a vapor cavity surrounded by a liquid. The balance of forces in Eq. (1) applied to the mid section of the bridge parallel to the substrates  $z^* = 0$  becomes

$$F^* = -\pi R_2^* \gamma_{lv}^* \left( 1 - \frac{R_2^*}{R_1^*} \right), \quad (2)$$

an expression which does not requires knowledge of the contact angle and  $R$ . According to this equation if  $R_1^* < 0$  the force is

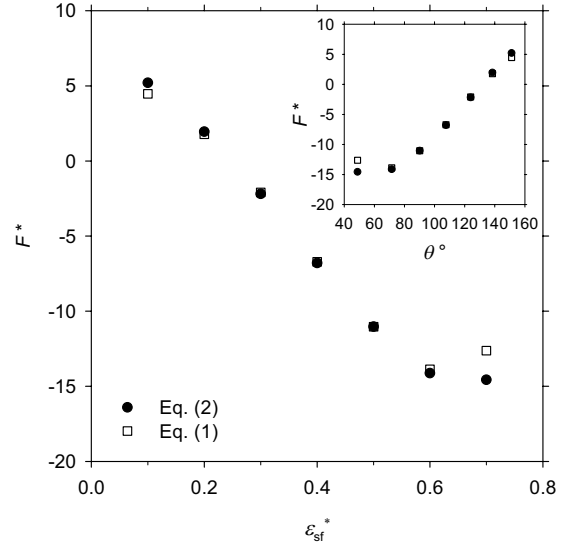


Figure 6: Force between substrates  $F^*$  due to a capillary bridge of liquid as function of the interaction parameter  $\epsilon_{sf}^*$  and as function of the contact angle  $\theta$  (inset). Calculations from Eq. (1) are at the triple-phase contact line and calculations from Eq. (2) are at the mid section of the bridge parallel to the substrates.

always attractive, but if  $R_1^* > 0$  the force can be attractive for  $R_1^* > R_2^*$  and repulsive for  $R_1^* < R_2^*$ . In the particular case of a sphere between the two solid surfaces, where  $R_1^* = R_2^*$ , the force is zero ( $\theta = 180^\circ$  for a bridge of liquid and  $\theta = 0^\circ$  for a vapor cavity). And in the case of a cylinder connecting the two surfaces, where  $R_1^* \rightarrow \infty$ , the force is attractive and given by  $F^* = -\pi R_2^* \gamma_{lv}^*$  ( $\theta = 90^\circ$ ). For the liquid bridges here, by

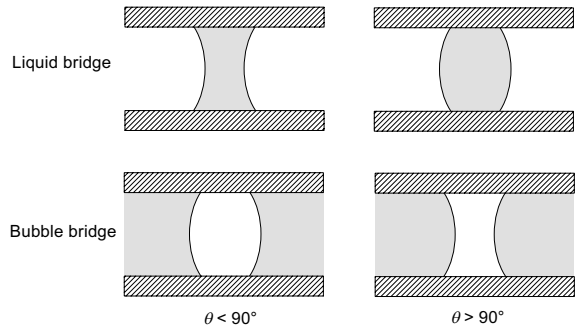


Figure 7: Schematic of liquid and bubble bridges for small and large contact angles.

using the curvature radii in Table 1 and the liquid-vapor interfacial free energy of  $\gamma_{lv}^* = 0.627$  at  $T^* = 0.68$  (this result is in good agreement with those of Vrabec *et al.* [20]), Eq. (2) provides an estimate for the vertical force acting between these two surfaces due to the capillary bridge in the same way as Eq. (1) though avoiding wetted area and contact angle parameters. The force for different values of  $\epsilon_{sf}^*$  applying Eq. (1) and Eq. (2) are coincident as Figure 6 shows. The force increases its attractive character as  $\epsilon_{sf}^*$  increases, or equivalently as  $\theta$  decreases,

although it is repulsive for  $\epsilon_{sf}^* < 0.2$ . The force for  $\epsilon_{sf}^* = 0.7$  is overpredicted from Eq. (1) since at this high wetting condition the circle does not describe well the bridge contour and consequently the values of the contact angle and  $R^*$ . Despite this the circle allows simple and accurate determination of the curvature radii  $R_1^*$  and  $R_2^*$  in the mid section of the bridge, and good estimations of contact angle and  $R^*$ . This macroscopic approach for the force is also valid for a capillary bridge generated by a cavity or a bubble. The force is mainly a function of the curvature radii. From the point of view of the application of Eq. (2), a capillary bridge of liquid at small contact angle is equivalent to a capillary bridge of a bubble at large contact angle (see Figure 7). In other words, if a liquid bridge generates high attraction between hydrophilic surfaces and repulsion between highly hydrophobic surfaces, a bubble bridge, surrounded by such a liquid, should generate high attraction between hydrophobic surfaces and repulsion between highly hydrophilic surfaces.

### 3.2.2. Non-equilibrium simulations

An alternative method to obtain the force between two solid substrates connected by a liquid bridge is through a simulation where the movement restrictions on the substrate are removed and the force at initial distance  $D^*(t^* = 0) = D_0^*$  is estimated from the initial acceleration  $a^*$  of the substrates. According to Newton's law  $F^*(t^*) = 2M^*d^2D^*(t^*)/dt^{*2} = 2M^*a^*$  with  $M^* = \sum_i m_{is}^*$  the mass of a substrate. Figure 8 shows the evolution of the distance between substrates  $D^*(t^*)$  for different values of the interaction parameter  $\epsilon_{sf}^*$ . For  $\epsilon_{sf}^* > 0.3$  the attraction

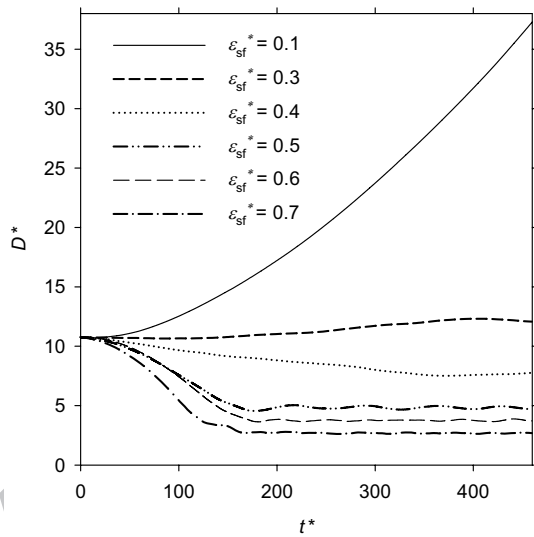


Figure 8: Evolution of separation distance  $D^*$  between substrates connected by a liquid bridge for different  $\epsilon_{sf}^*$  at  $T^* = 0.68$ .

between the substrates increases as  $\epsilon_{sf}^*$  increases and the equilibrium distance between them diminishes. For  $\epsilon_{sf}^* < 0.3$  the surfaces separate from each other because the repulsion is higher than the attraction from the surface tension force. For  $\epsilon_{sf}^* > 0.8$  the interactions between substrate and fluid particles are high enough to destabilize the liquid bridge and thus the only force

that remains after the capillary breaks is due to the vapor between the substrates, which is repulsive. In all these previous cases, an immediate response to the perturbation is followed by an oscillatory behavior until the fixed point is reached. For  $\epsilon_{sf}^* = 0.3$  and  $0.4$  it is interesting to notice that the oscillatory behavior is barely seen in Figure 8 because near the critical  $\epsilon_{sf}^*$  at which the force between the substrates changes from attractive to repulsive, the dynamics become much more slow. Relative acceleration of the substrates  $a^*$  is computed from a quadratic fit to the distance between substrates  $D^*(t^*) = D_0^* + v_0^*t^* + 0.5a^*t^{*2}$  immediately after releasing them, between  $t^* = 0$  to  $t^* = 46$ . During this period of time the acceleration is nearly constant for every value of  $\epsilon_{sf}^*$ . The vapor between the substrates exerts a pressure, small at  $T^* = 0.68$ , that is not compensated on the empty region between the external faces of the substrates. We estimate this force contribution for  $\epsilon_{sf}^* = 0.8$  for which there is no bridge in the equilibrium configuration. This small force once subtracted from the force obtained from the  $D^*(t^*)$  curves gives the force from the bridges. Similar results for the force exerted by the vapor on the substrates were obtained considering it as ideal gas. Here we also calculate the force due to a liquid bridge from the relative velocity of the center of mass of each substrate once their movement restriction is removed. To obtain the acceleration in this case we use a linear fit of the instantaneous relative velocity between substrates  $v^*(t^*)$  in the time interval  $t^* = 0$  to  $t^* = 46$ . As expected, these two approaches lead to results that are in excellent agreement as Figure 10 shows.

### 3.2.3. Integration of normal pressure radial profile

Yet another way to calculate the force between the substrates due to the presence of the liquid bridge is from the net force across a hypothetical plane parallel to the substrate. This force is the result of particle interactions whose action line crosses the plane and of every collision of particles with this surface and it can be estimated by integration of the normal component of the pressure tensor profile  $P_N^*(r^*, z^*)$  inside the bridge along the  $r$ -coordinate for a given plane  $z^*$ . The normal component of the local pressure tensor is calculated according to the Irving-Kirkwood formalism [18, 19]. For simplicity we evaluate the force in the middle of the bridge, plane  $z^* = 0$ , through numerical integration by

$$F^*(z^* = 0) = \int_0^{r^*} P_N^*(u, z^* = 0) 2\pi u du. \quad (3)$$

Integration in Eq. (3) is from the center axis of the bridge at  $r^* = 0$  to  $r^*$  at which the density is that of the bulk vapor phase. The repulsive force due to the vapor surrounding the liquid bridge is not taken into account because we are interested just in the force due to the liquid bridge. The kinetic  $P_N^{K*}$  and virial  $P_N^{U*}$  contributions at  $z^* = 0$  are shown in Figure 9 for different values of  $\epsilon_{sf}^*$ . It is the balance between these two terms which determines the repulsive or attractive character of the force due to the bridge; while the kinetic term is always repulsive, the virial term sets the attractive contribution which increases at the liquid-vapor interface. The kinetic term of the pressure tensor inside the bridge is unaffected by  $\epsilon_{sf}^*$ , but the virial component inside the bridge is increasingly negative or attractive when  $\epsilon_{sf}^*$

increases. For  $\epsilon_{sf}^* = 0.1$ , on average, the kinetic term exceeds the virial term, leading to a repulsive force between the substrates. For  $\epsilon_{sf}^* = 0.7$  the result is the opposite. Figure 10 shows

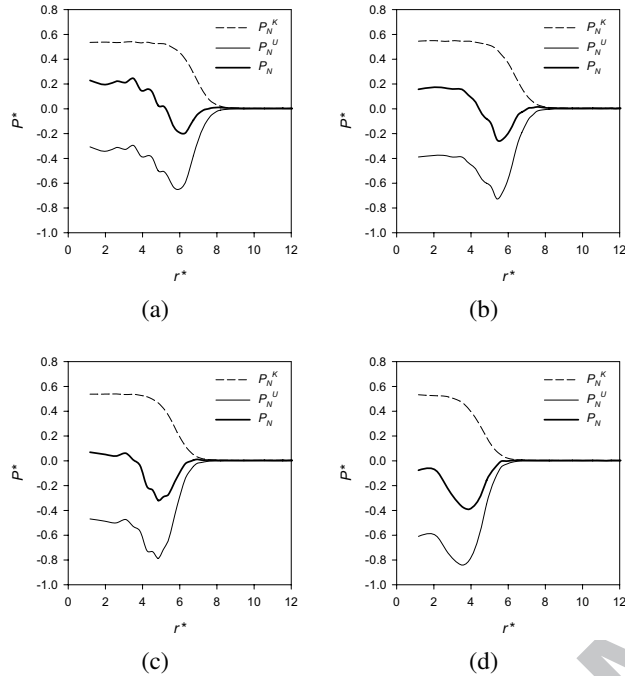


Figure 9: Radial profiles of the normal pressure component at the contact surface  $z^* = 0$ .  $P_N^{K*}$  and  $P_N^{U*}$  correspond to the kinetic and virial components of the normal component of the pressure tensor  $P_N^*$ . Results are for  $T^* = 0.68$ ,  $N_f = 941$  and different  $\epsilon_{sf}^*$  (a) 0.1, (b) 0.3, (c) 0.5 and (d) 0.7.

the force between two substrates due to a capillary bridge as a function of  $\epsilon_{sf}^*$  predicted from the various methods described above. The force estimated from non-equilibrium simulations where the substrates are free to move are in agreement with the force predicted from the macroscopic force balance, Eqs. (1) and (2) and with the force predicted from the integration of the normal pressure radial profile of equilibrated bridges (Eq. 3). According to Figure 10 the force due to a liquid bridge is attractive even when the substrates are only moderately wetted by the liquid, including values of  $\epsilon_{sf}$  as low as 0.25. For cavities the force is attractive even when the substrates are moderately solvophilic. From a molecular point of view it is important to notice that even for a Lennard-Jones potential, where the repulsive and attractive contributions vanish at distances comparable to the particle diameter, the much larger range of the force between the substrates is a collective phenomenon. We believe that the present methodology when applied to water as the intervening liquid between the substrates, should lead to a better understanding of unexpected long range attractive forces, probably due to capillary bridging, that have been measured between hydrophobic surfaces, see for instance [21–26], in non-symmetrical hydrophilic-hydrophobic systems in saline solutions, see for instance [26–36], and even more recently in partially hydrophilic surfaces in electrolyte solutions [37–39].

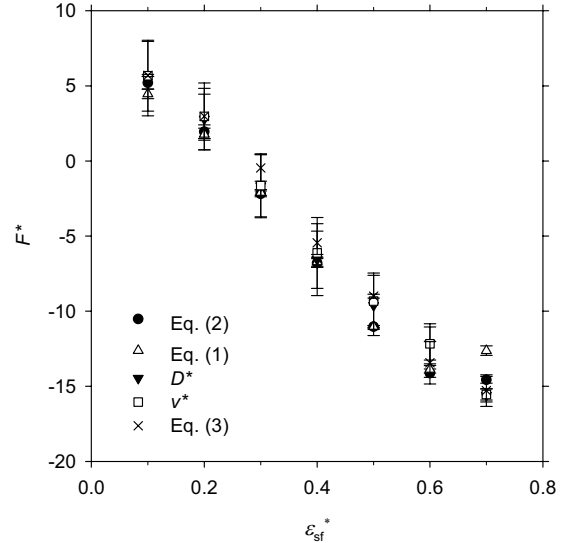


Figure 10: Force between substrates due to a liquid bridge for different  $\epsilon_{sf}^*$ . Comparison of predictions from (i) macroscopic force balance (Eqs. 1 and 2) with parameters from molecular simulations, (ii) Newton's second law applied to the free advance of the surfaces and obtained from the evolution of the distance between substrates  $D^*$  and the relative substrates velocity  $v^*$  and (iii) integration of the radial profile of normal pressure inside the liquid capillary bridge (Eq. 3). Results correspond to averages over three realizations of each simulation.

#### 4. Conclusions

Molecular dynamics simulations allow the study capillary liquid bridges between two planar substrates and the resulting force between them. Different wettability degrees are set by varying the fluid-solid interaction parameter. Contact angle at the triple-phase contact line measured through the liquid phase decreases as the interaction parameter increases. We present force estimates from (i) macroscopic force balance with parameters from molecular simulations, i.e., liquid-vapor interfacial free energy, radii of curvature and wetted area of the bridge, and contact angle at the triple-phase contact line, (ii) Newton's second law applied to the free advance of the substrates mediated by the liquid bridge, and (iii) integration of the normal pressure radial profile inside the bridge. Good agreement is generally observed between the different methods. There is a threshold value for the fluid-substrate interaction parameter for which the substrates separate instead of joining ( $\epsilon_{sf}^* = 0.25$ ) and another threshold value for which the capillary bridge becomes mechanically unstable and breaks into droplets ( $\epsilon_{sf}^* > 0.70$ ). For liquid bridges the force is attractive when the substrates are solvophilic and even when the substrates are moderately solvophobic; and thus for cavities surrounded by the same liquid the force is attractive even when the substrates are moderately solvophilic.

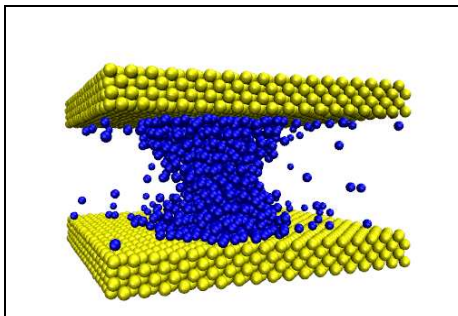
#### Acknowledgements

We thank Project Conicyt/Fondecyt 1101023, Centro CRHIAM Project Conicyt/Fondap-15130015 and Red Doctoral

REDOC.CTA, MINEDUC Grant #UCO1202 for financial support. J.H.S. thanks University of Concepción, CONICYT, and Mecesp for graduate student fellowships.

## References

- [1] J. Koplik, J.R. Banavar, J.F.Willemsen, *Phys. Fluids A* **1** (1989) 781.
- [2] B. Busic, J. Koplik, J.R. Banavar, *J. Non-Newtonian Fluid Mech.* **109** (2003) 51.
- [3] J. Koplik, J.R. Banavar, *Phys. Rev. E* **67** (2003) 011502.
- [4] K. Bucior, L. Yelash, K. Binder, *Phys. Rev. E* **79** (2009) 031604.
- [5] S. Maruyama, T. Kurashige, S. Matsumoto, Y. Yamaguchi, T. Kimura, *Microscale Thermophys. Eng.* **2** (1998) 49.
- [6] S. Maruyama, T. Kimura, M.-C. Lu, *Thermal Sci. Eng.* **10** (2002) 23.
- [7] B. Shi, V.K. Dhir, *J. Chem. Phys.* **130** (2009) 034705.
- [8] F. Leroy, F. Müller-Plathe, *J. Chem. Phys.* **133** (2010) 044110.
- [9] D.T. Semiroimi, A.R. Azimian, *Heat Mass Transfer* **47** (2011) 579.
- [10] E.M. Grzelak, J.R. Errington, *J. Chem. Phys.* **128** (2008) 014710.
- [11] E.M. Grzelak, J.R. Errington, *J. Chem. Phys.* **132** (2010) 224702.
- [12] K.S. Rane, V. Kumar, J.R. Errington, *J. Chem. Phys.* **135** (2011) 234102.
- [13] V. Kumar, J.R. Errington *J. Chem. Phys.* **139** (2013) 064110.
- [14] S.K. Das, K. Binder, *EPL* **92** (2010) 26006.
- [15] L. Verlet, *Phys. Rev.* **159** (1967) 98.
- [16] A. Trokhymchuck, J. Alejandre, *J. Chem. Phys.* **111** (1999) 8510.
- [17] F.H. Stillinger, *J. Chem. Phys.* **38** (1963) 1486.
- [18] J.H.Irving, J.G. Kirkwood, *J. Chem. Phys.* **18** (1950) 817.
- [19] J.P. Walton, D.J. Tildesley, J.S. Rowlinson, J.R. Henderson, *Mol. Phys.* **48** (1983) 1357.
- [20] J. Vrabc, G.K. Kedia, G. Fuchs, H. Hasse, *Mol. Phys.* **104** (2006) 1509.
- [21] E. Kokkoli, C.F. Zukoski, *J. Colloid Interface Sci.* **230** (2000) 176.
- [22] G.E. Yakubov, H.-J. Butt, O.I. Vinogradova, *J. Phys. Chem.* **104** (2000) 3407.
- [23] T. Ederth, K. Tamada, P.M. Claesson, R. Valiokas, R. Jr., Colorado, M. Graupe, O.E. Shmakova, T.R. Lee, *J. Colloid Interface Sci.* **235** (2001) 391.
- [24] O.I. Vinogradova, G.E. Yakubov, *J. Chem. Phys.* **114** (2001) 8124.
- [25] J.W.G. Tyrrell, P. Attard, *Langmuir* **18** (2002) 160.
- [26] C.S. Hodges, J.A.S. Cleaver, M. Ghadiri, R. Jones, H.M. Pollock, *Langmuir* **18** (2002) 5741.
- [27] S.M. Acuña, P.G. Toledo, *Langmuir* **24** (2008) 4881.
- [28] S.M. Acuña, P.G. Toledo, *J. Colloid Interface Sci.* **361** (2011) 397.
- [29] Ya.I. Rabinovich, R.-H. Yoon, *Langmuir* **10** (1994) 1903.
- [30] M. Mantel, Ya.I. Rabinovich, J.P. Wightman, R.-H. Yoon, *J. Colloid Interface Sci.* **170** (1995) 203.
- [31] O. Teschke, E.F. de Souza, *Langmuir* **19** (2003) 5357.
- [32] O. Teschke, E.F. de Souza, *Chem. Phys. Lett.* **375** (2003) 540.
- [33] S.M. Acuña, M.A. Sánchez, P.G. Toledo, *Int. J. Nanosci.* **3** (2004) 499.
- [34] E.E. Meyer, Q. Lin, T.Hassenkam, E. Oroudjev, J.N. Israelachvili, *PNAS* **102** (2005) 6839.
- [35] S.M. Acuña, P.G. Toledo, *Maderas : Ciencia y Tecnología* **12** (2010) 209.
- [36] J.H. Saavedra, S.M. Acuña, P.G. Toledo, *J. Colloid Interface Sci.* **410** (2013) 188.
- [37] D.T. Atkins, P. Kékicheff, O. Spalla, *J. Colloid Interface Sci.* **188** (1997) 234.
- [38] H. Guleryuz, A.K. Royset, I. Kaus, C. Filiâtre, M.-A. Einarsrud, *J. Sol-Gel Sci. Technol.* **62** (2012) 460.
- [39] P. Troncoso, J.H. Saavedra, S.M. Acuña, R. Jeldres, F. Concha, P.G. Toledo, *J. Colloid Interface Sci.* accepted.



Molecular dynamics simulation of a capillary liquid bridge (blue) equilibrated between two identical surfaces (yellow) for a given temperature. Particle interactions in the fluid and in the substrates are modeled with the 12-6 Lennard-Jones potential. Variable well depths for the substrate-fluid particle interaction are used to attain different wetting conditions. The force between the substrates is obtained from a macroscopic force balance and from simulation data.

ACCEPTED MANUSCRIPT

- MD simulations are used to study capillary liquid bridges between flat substrates
- And also the origin, strength and range of the resulting force between them
- Pairwise interactions are described by the Lennard-Jones potential
- Wettability is tuned by varying the fluid-solid well depth interaction parameter
- Force is attractive when the substrates are solvophilic or moderately solvophobic

ACCEPTED MANUSCRIPT